Chemical Physics 572 (2023) 111953

Contents lists available at ScienceDirect

Chemical Physics

journal homepage: www.elsevier.com/locate/chemphys

Phase equilibria and structure of inhomogeneous logarithmic fluids: An atomistic simulation study

Madison Lasich [a,*], Konstantin G. Zloshchastiev [b]

[a] Department of Chemical Engineering, Mangosuthu University of Technology, Durban 4031, South Africa
[b] Institute of Systems Science, Durban University of Technology, Durban 4000, South Africa

ARTICLE INFO

Keywords:
Phase equilibrium
Viscosity
Pair potential
Molecular physics

ABSTRACT

Monte Carlo and molecular dynamics simulations are applied to study the phase equilibria and structure of a fluid described by a logarithmic interparticle potential. The two-phase pure species phase envelope was generated for various values of the size term of the potential, and the critical point (the set of conditions at which both phases became indistinguishable) was estimated in each case. A monotonic relationship between both the reduced critical density and temperature and the size term was demonstrated. Molecular dynamics simulations were employed to study the influence of the thermodynamic conditions on the fluid structure, and three different fluid structures were elucidated.

1. Introduction

Wave equations containing logarithmic nonlinearity have found useful application in various branches of physics such as nuclear physics, condensed-matter theory, particle physics, physical vacuum theory, and quantum gravity, to mention few literature landmarks [1–19]. Such a diversity can be explained by the fact that for many-body systems, the logarithmic nonlinearity occurs as a leading-order approximation if their interaction energies predominate kinetic ones [12]. Examples of such systems include low-temperature quantum Bose liquids [11,14,15,18] and also Korteweg-type materials where capillarity and surface tension play significant roles [7,13,17,19]. In the corresponding models, liquid–solid or vapour–liquid phase transitions can occur, which makes them useful descriptions of flows taking place in the presence of interface and surface effects [20,21].

One prediction of the theory is large-scale periodical density inhomogeneities, caused by the existence, in the vicinity of a liquid–solid phase transition, of multiple Gaussian-shaped solitary wave solutions for an underlying logarithmic wave equation. Recently, a study of these solutions' application was done for geophysical silicate materials, such as magmas in volcanic conduits or polycrystalline metals [13,19].

The occurrence of the Gaussian-shaped density inhomogeneities indicates that they can become independent dynamical objects hence there are new degrees of freedom. Therefore, the correct theory would be the one formulated in terms of these objects.

Several different real systems can be described as particles interacting with a pair potential containing a term which is proportional to the constituent particles' logarithm. For example, the electrostatic interaction energy between two charges [22] and the interparticle potential in superfluid helium [11] can all be described in this manner.

Previously, Monte Carlo simulations were employed to study a model fluid with a logarithmic pair potential [23], and it was confirmed that predictions [24] regarding the calculation of the internal energy using standard statistical mechanics were acceptable. In the present study, a potential originally devised for describing superfluid phase of helium-4 [11] – a system with significant capillarity – is employed in Monte Carlo and molecular dynamics simulations to study more general features of this type of fluid, such as phase equilibria and fluid structure.

The influence of the pair potential's size term in the (which is described in the subsequent section) on the phase equilibria of pure species is discussed, including an investigation of the effect of this term on the critical point (the thermodynamic conditions at which the lighter and denser phase become indistinguishable). In addition, structural transitions in the fluid are investigated using molecular dynamics, in which it is demonstrated that there may be up to three distinct fluid structures present, depending on the thermodynamic conditions. Furthermore, comparison is drawn with other systems from the literature, namely aggregates in magma and collapsing disks, which exhibit qualitatively similar behaviour.

2. Interactions in inhomogeneous logarithmic fluid

A brief introduction into the logarithmic fluid models can be found in Refs. [11,13,14] where it is shown that in a cellular phase the density

* Corresponding author.
E-mail addresses: lasich.matthew@mut.ac.za (M. Lasich), kostiantynz@dut.ac.za, kostya@u.nus.edu (K.G. Zloshchastiev).

https://doi.org/10.1016/j.chemphys.2023.111953
Received 15 August 2022; Received in revised form 16 March 2023; Accepted 4 May 2023
Available online 9 May 2023

of a system in the ground (energetically favourable) state is described by a Gaussian function, and therefore a logarithmic fluid tends to inhomogenize itself into lumps. The latter can serve as new degrees of freedom, such as fluid parcels (volume elements) which are widely used in a hydrodynamic approach. Such objects not only have a finite size, of order a, but also interact with each other. Altogether, it means that one has to separately derive an inter-particle ("inter-parcel") potential, which would encode not only interactions between fluid parcels but also their finite size.

Moreover, for simplicity and technical reasons, such a potential can have a two-body interaction, at least in a leading-order approximation. In this picture, fluid parcels can be regarded as pairwise-interacting point particles. The energy of such interactions can be derived from energy arguments.

Using the Gaussian form of the solution, one can obtain [11] that a Gaussian volume element of size $r \sim a$ stores an amount of internal bulk mass-energy, which is proportional to

$$\int_0^r \rho_g(r')r'^2 dr' \propto \frac{1}{a}(r-r_0)\,\mathrm{e}^{-(r/a)^2}\left[1+\mathcal{O}(r-a)\right], \tag{1}$$

where r is an inter-particle separation, and the value

$$r_0 = a\left[1/2 + 1/(\mathrm{e}\sqrt{\pi}\,\mathrm{erf}(1))\right] \approx 0.75\,a, \tag{2}$$

refers to the point where the dominant term of $\epsilon(r)$ changes sign.

Furthermore, each fluid parcel is known to be stable with respect to small perturbations [10], therefore it tries to maintain its size and mass. Consequently, in order to change the latter values, an amount of energy must be supplied which is proportional to the expression (1). In the absence of other fields, this energy can come only through interaction with other fluid parcels, therefore one can conclude that

$$U(r) = \frac{U_0}{a}(r-r_0)\,\mathrm{e}^{-r^2/a^2}, \tag{3}$$

up to the terms of order $\mathcal{O}(r-a)$. Note that r here is, in practice, the interparticle separation.

The latter can be assumed small unless interactions deform fluid parcels so strongly that their interior structure cannot be neglected. However, under those conditions we would fall outside the range of applicability of a hydrodynamic approach as such. Here, the proportionality factor $U_0 = -aU(0)/r_0 \approx -1.34\,U(0)$ becomes the free parameter of the hydrodynamic model. In this context, the critical value r_0 determines the inter-parcel separation at which the potential switches between attraction and repulsion.

The expected structural features of a fluid described by this potential energy function include a well-defined interparticle separation at the minimum of the potential energy, which can lead to a more ordered structure than fluids with weaker or less defined interaction potentials. At larger separations, the potential energy decays exponentially with distance, which may lead to a shorter range of correlations in the fluid than for other interaction potentials that have a longer-ranged repulsion or attraction. The pair potential of this fluid is contrasted with that of a comparable Lennard-Jones fluid in Fig. 1.

At low temperatures, the fluid is expected to form a condensed phase due to the attractive well of the potential energy. The properties of the condensed phase, such as the density and the correlation functions, depend on the well depth U_0 and the position of the minimum of the potential energy r_0. At high temperatures, the fluid may exhibit a vapour phase, with a vapour–liquid phase transition at a critical temperature and density, depending on the parameters U_0, r_0, and a.

3. Methods

In this section we describe numerical methods which are going to be used. The inter-parcel two-body potential (3) is implemented using a tabulated potential, with its value computed at 1000 discrete points over the range 0 nm $\leq r \leq$ 1.85 nm. Interpolation between tabulated values was effected using a cubic spline. Following the minimum-image convention [25], a cut-off radius of 1.5 nm was employed in all simulations.

3.1. Monte Carlo simulation

Stochastic Monte Carlo (MC) simulations in the isochoric-isothermal Gibbs ensemble [26,27] were performed for systems comprising 1000 particles distributed across two phases, defined by their nominal density, using the Metropolis scheme [28] and MCCCS Towhee software [29]. Simulations were run for up to 10,000 MC cycles to achieve equilibrium (typically equilibrium was reached within 2000 MC cycles), following which up to 10,000 MC cycles were used to generate acceptable results with averages computed using block averages for runs divided over 5 blocks. Note that an MC cycle is a number of moves equal to the number of particles in the system. The following MC moves were considered (with their relative occurrences in brackets): particle exchange between phases (39.5%), particle translation (30.0%), particle exchange within a phase (30.0%), and volume exchange [30] (0.5%). In terms of real-world phenomena, particle exchange between phases mimics mass transfer between phases, particle translation and exchange within a phase mimic the thermal motion of particles within a phase, and volume exchange corresponds to an isotropic volume adjustment.

MC molecular simulation essentially generates a set of atomistic configurations sampled from the desired ensemble, with each configuration being used to generate the next one in turn. The simulation proceeds as follows: Firstly, a trial configuration m is generated for which its energy computed, then this trial configuration is compared to the original configuration n, and if the new configuration m possesses a lower energy it is accepted, while if it does not, then the chance to be accepted is P_{mn}:

$$P_{mn} = \min\left[1, \frac{p_n}{p_m}\right], \tag{4}$$

wherein p represents the probability of each configuration.

For the MC simulations, equilibrium between phases was studied by initializing one phase as the dense phase and the other as a lighter one; with 750 particles and 250 particles in each phase, respectively. The parameter r_0 was varied, to develop a set of temperature and phase density values for each value of r_0. In each case, a critical point can potentially form at which the two phases are indistinguishable in terms of density. During the course of the production stage, configurations were sampled every 5000 Monte Carlo steps in order to generate data.

3.2. Molecular dynamics simulation

Dynamic simulations were undertaken in the canonical (i.e. isochoric-isothermal) ensemble using 1000 particles in a single phase with a time step of 1 fs. The bulk density was fixed at that corresponding to superfluid Helium (i.e. $\rho = 0.145$ kg/m^3). The simulation cells for the dynamic simulations were generated using random placement by employing the classical COMPASS forcefield [31] applied to helium to obtain a density equal to superfluid helium (i.e. 0.145 g/mL). Next, the simulation was allowed to proceed for 100 ps with the imposed logarithmic fluid pair potential. Then, each system was equilibrated using the Nosé–Hoover–Langevin thermostat [32] for up to 2 ns. Next, results were generated over by sampling every 50 fs over the course of a further 2 ns using the Nosé–Hoover–Langevin thermostat. Typically simulations reached equilibrium within 100 ps, but for the sake of rigour additional simulation time was permitted as this pair potential has not been studied before using molecular dynamics. To integrate the equations of motion, the Verlet velocity integrator scheme [33] was used. All molecular dynamics simulations were performed using the Materials Studio 2018 computer programme package [34].

Two properties of the system were studied in depth using molecular dynamics simulations: Radial distribution function, and self-diffusion coefficient. The self-diffusion coefficient was computed by considering the slope of the mean squared displacement of the particles over the

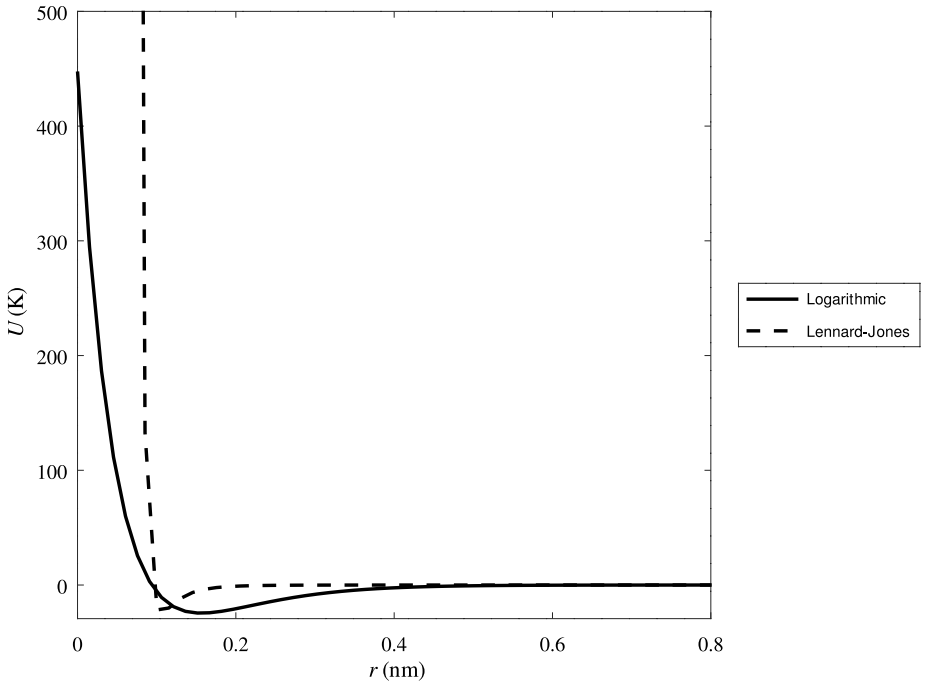

Fig. 1. Interparticle potential energy for a fluid described using the logarithmic pair potential as versus a comparable Lennard-Jones fluid.

course of the production runs according to the Einstein equation [35, 36]:

$$D = \frac{1}{6} \lim_{\Delta t \to 0} \frac{d(MSD)}{d(\Delta t)} \tag{5}$$

Configurations were sampled every 5 ps to generate data during the production stage of the molecular dynamics simulations. Only the linear region of the MSD curve was used to compute the diffusion coefficient, which typically ran up to 1.5 ns. The uncertainty in the diffusion coefficient was computed by estimating fluctuations over the course of the simulation time [37].

4. Results

4.1. Monte Carlo simulations

Fig. 2 shows the results of the two-phase MC simulations, wherein there is a shift towards higher densities for both phases as the value of the parameter r_0 increases. In every case, a critical point developed at which the two phases became indistinguishable in terms of density for a specific temperature value. As the value of r_0 increased, this critical point shifted towards downwards lower temperatures. Earlier work on systems of collapsing hard disks with a repulsive interparticle interaction coupled with a square well potential [38] may provide a helpful comparison to describe the behaviour observed here. Increasing the width of the repulsive step produced a qualitatively similar effect in the low density region of the phase diagram for hard disks as compared to decreasing the size term used in the present study's pair potential, in terms of shifting the phase envelope from high density and low temperature towards lower density and higher temperature.

The locus of the critical point is presented in Fig. 3, illustrating the effect that the particle size term r_0 has on both the temperature and density at the critical point. While the dimensionless density increased quickly with respect r_0, this did not hold when the density was considered in dimensional terms in which case the critical density was constant at about 0.008 g/cm^3 in all cases. The critical temperature was strongly influenced by the particle size, as evidenced by its rapid decrease with increasing r_0.

In order to probe the structure of the fluid, molecular dynamics simulations were performed to sample configurational data in order to generate the radial distribution function of the fluid. A highly ordered substance, such as a crystal, would have many clear distinct peaks in the radial distribution function, indicating regular placement of molecules within the supramolecular structure. In contrast, a homogeneous fluid with no order whatsoever, such as an ideal gas, would not have any notable peaks in the radial distribution function, suggesting that it may not be likely that particles are not generally pinned down in relation to each other and tend to circulate freely and randomly. The results of this analysis into the fluid structure are explained in the next section.

4.2. Molecular dynamics simulations

Molecular dynamics simulations were undertaken at a fixed density of $\rho* = 0.018$ (corresponding to a density of 0.145 g/mL, the density of superfluid helium) to study the influence of temperature on the fluid structure. These results are presented in Fig. 4 in the form of the radial distribution function of the fluid as a function of temperature. The data appear to suggest that two structural transitions occur, namely in the regions $0.323 < T* < 0.129$ and $1.67 < T* < 2.26$. At low temperatures (i.e. $T* < 0.129$) the fluid appears to possess a notable degree of supramolecular order, as evidenced by the presence of two distinct peaks in the radial distribution function, at around $r/r_0 = 1.5$ and $r/r_0 = 0.71$. As the temperature is increased from past $T* = 0.0168$, the fluid becomes more disordered and homogeneous, as the second outer peak in the radial distribution function disappears and is replaced by a single broad peak, suggesting a supramolecular structure reminiscent of a classical Lennard-Jones fluid. This first transition is not evident in the phase diagram shown in Fig. 2, suggesting that it is a transition from one liquid phase to another. At temperatures above $T* = 3.23$, the fluid becomes almost completely homogeneous, with the single broad peak present in the region $0.0168 < T* < 1.375$ being replaced by an essentially flat non-zero radial distribution function. This high temperature regime suggests little to no regularity or order in the fluid structure, as may be found in an ideal fluid. With reference to the phase diagram presented in Fig. 1, this high temperature transition

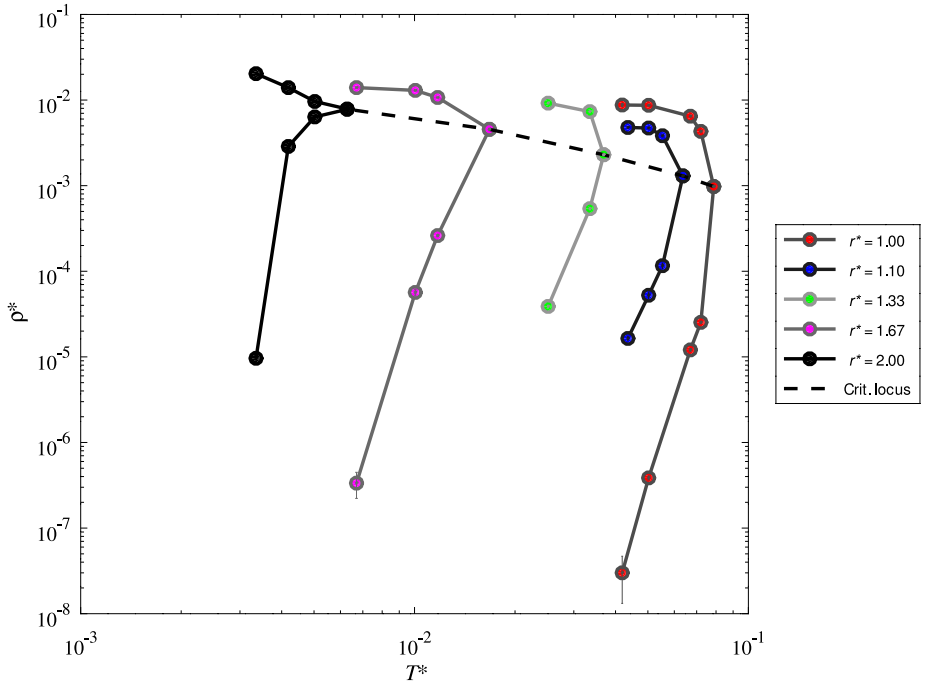

Fig. 2. Phase diagram generated by two-phase MC simulations for a logarithmic condensate. Note that the horizontal axis has been made logarithmic for clarity. Note that $r* = \frac{r_0}{r_0^{ref}}$ wherein r_0^{ref} is the reference case from the literature [11]. $T*$ is the dimensionless temperature $\frac{T}{U_0}$ and $\rho*$ is the dimensionless density $\frac{\rho V}{N r_0^3}$.

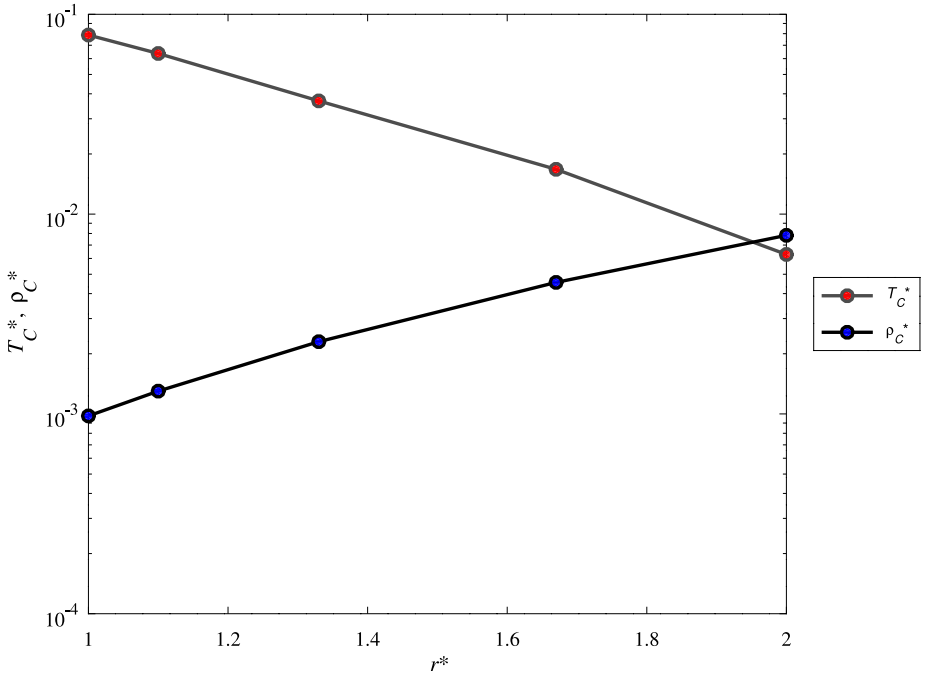

Fig. 3. Locus of the critical point of the two-phase logarithmic condensate as the particle size term r_0 is increased. Note that $r* = \frac{r_0}{r_0^{ref}}$ wherein r_0^{ref} is the reference case from the literature [11]. T_C* is the dimensionless critical temperature $\frac{T_C}{U_0}$ and ρ_C* is the dimensionless critical density $\frac{\rho_C V}{N r_0^3}$.

corresponds with the critical temperature of the fluid, suggesting that the supercritical form of this fluid is very close to an ideal gas in terms of supramolecular structure and behaviour.

The RDF of a liquid with multiple peaks indicates that the particles in the liquid are organized in a non-uniform manner, with certain distances between particles being more favourable than others. The presence of multiple peaks in the RDF suggests that the liquid has some degree of order, which can arise from interactions between the particles. In particular, the presence of multiple peaks can indicate the presence of local structure or clustering in the liquid. In contrast, a liquid with dispersive van der Waals forces would have a more uniform RDF, indicating a more homogeneous distribution of particles throughout the liquid. A high density within small "parcels" of fluid suggests the presence of strong intermolecular forces, which tend to pull the particles together and lead to a more tightly packed structure. This can also contribute to the formation of local structures and the

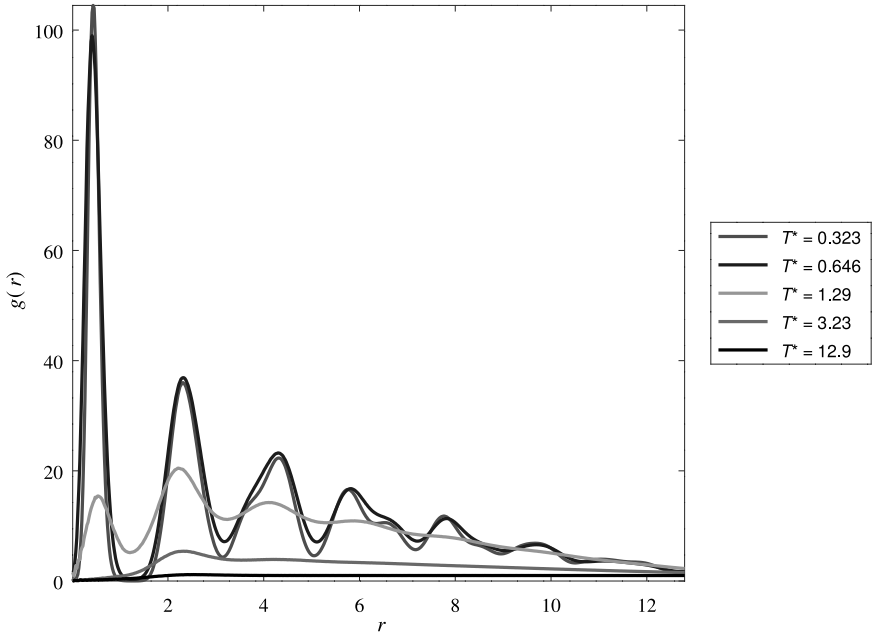

Fig. 4. Radial distribution function as a function of temperature at constant density. Note that $T* = \frac{T}{U_0}$.

presence of multiple peaks in the RDF. Overall, the structural features of a liquid with multiple peaks in its RDF and a high density within small "parcels" of fluid suggest the presence of strong, directional interactions between particles in the liquid, which can give rise to local order and structure.

In terms of fluids examined in the literature, comparison with magnetite-bubble aggregates in andesite magma (shown in Fig. 5) may be instructive [39]. In this regard, the low temperature regime observed in the present study presents some qualitative similarities with the completely randomized magnetite-bubble aggregates, albeit with a larger degree of structure than magma (as evidenced by the order of magnitude differences in the values of $g(r)$). This is somewhat unexpected, as typically fluids take on more orderly arrangements as thermal motion decreases. At moderate temperatures, there is a qualitative resemblance to randomized magnetite-bubble aggregates with weak clustering, although as with the low temperature regime, the fluid in this study displays notably more structure than magma. This transition from complete randomness to weak clustering is unexpected for the thermal motion reasons described above. A possible behaviour that may be related to such behaviour is the transition from liquid to vapour, by which the moderate temperature regime resembles a nascent 'vapour' nucleation regime, by which the weak clustering is in effect a prelude to the formation of 'vapour' bubbles within the denser 'liquid' phase and represents possible regions which are more likely to undergo phase transition first.

As part of investigating structural transitions, the self diffusion coefficient was computed as a function of temperature (following the approach of Einstein [35] described above) as shown in Fig. 6. In this analysis there appear to be two different fluid regimes. Firstly, at low temperatures (below $T* = 1.29$) the diffusion coefficient is effectively independent of temperature. A transition occurs at around this temperature, however, resulting in a fluid for which the diffusion coefficient increases rapidly as a function of temperature. In this high temperature region, the fluid may behave similarly to a classical rarefied gas, since D is roughly proportional to T^{frac23}. The low diffusion coefficient at low temperature temperatures can be related to the structure observed in the RDFs presented in Fig. 4, wherein it was observed that the logarithmic fluid possesses significant supramolecular structure under these conditions. This orderly structure was fairly persistent with respect to changes, until a transition was observed around $T* = 1.29$. Hence, it would appear that the logarithmic fluid forms parcels of fluid with high local density that are resistant to thermal changes up to the point at which transition to a rarefied gas occurs. This behaviour at low temperature concurs qualitatively with the analysis of expected fluid structure presented earlier in this contribution.

With regard to the moderate temperature phase, the nature of the fluid may be further divided into two regions, based on the diffusion behaviour. At higher temperatures within the moderate temperature range (i.e. $0.670 < T* < 1.675$), the fluid exhibits an Arrhenius temperature dependence (i.e. $\log D \propto -\frac{1}{T}$), suggesting that it behaves as a viscous fluid as the temperature is increased towards the transition into the rarefied classical gas present at high temperatures. However, in the lower range of the moderate temperature range (i.e. $0.0168 < T* < 0.670$), it unclear what behaviour dominates. Comparing the diffusion coefficient with temperature suggest that the fluid may behave somewhat like a rarefied gas since $D \propto T^{\frac{2}{3}}$, although this trend is not fully linear, thus moderating any conclusions about this behaviour.

5. Conclusions

Monte Carlo and molecular dynamics simulations were performed using a fluid with the interparticle potential (3). Notably, this particular form of potential has occurred in inhomogeneous logarithmic liquid models and has been previously used to describe microscopic structure of the superfluid phase of helium-4 [11]. In this paper, we studied properties of the fluid with this potential at a classical statistical mechanics level.

Monte Carlo simulations were employed to study the phase behaviour of the fluid whilst varying both the temperature and the size terms in the interparticle potential, and it was observed that there is a monotonic relationship between the size term and both the critical density and temperature of the fluid. Criticality in this context refers to the point (T, ρ) at which the two phases of the fluid become indistinguishable in terms of density, in a condition analogous to that found in a classical fluid.

Molecular dynamics simulations yielded insights into the fluid structure, and suggested that there may in fact be two structural regimes for the fluid, depending on the thermodynamic conditions. The structural regimes were classified according to the number of distinct shells in the radial distribution function of the fluid. Analysis of the self-diffusion

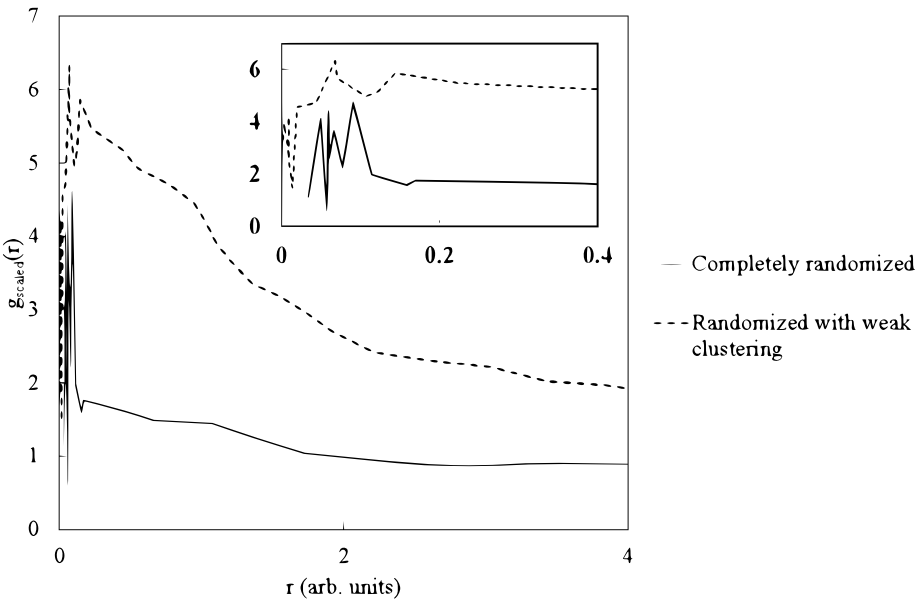

Fig. 5. Radial distribution function for magnetite-bubble aggregates in andesite magma [39] with inset focusing on the region $r \leq 0.4$.

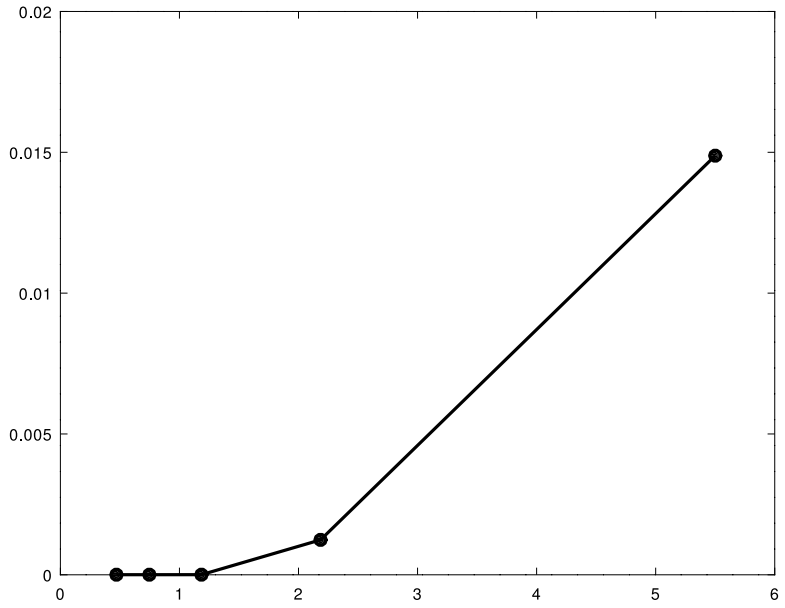

Fig. 6. Diffusion coefficient D as function of temperature. $T*$ is the dimensionless temperature $\frac{T}{U_0}$.

coefficient of the fluid confirmed the presence of the different fluid structures. Understanding the role that the thermodynamic conditions play in altering the structure of the fluid may be helpful in other applications of the logarithmic pair potential discussed above.

Finally, a comparison was made with systems of collapsing disks and aggregates in magma, for which qualitatively similar behaviours were observed. In the case of the former, the width of a repulsive interparticle interaction was found to influence the phase diagram in an inverse manner to the effect of the size term in the present work. For the latter system, there are structural similarities for the different fluid regimes to different phases of bubble aggregates in magma.

CRediT authorship contribution statement

Madison Lasich: Conceptualization, Data curation, Formal analysis, Methodology, Project administration, Resources, Software, Supervision, Validation, Visualization, Writing – original draft, Writing – review & editing. **Konstantin G. Zloshchastiev:** Conceptualization, Data curation, Formal analysis, Methodology, Project administration, Supervision, Validation, Writing – original draft, Writing – review & editing.

Declaration of competing interest

The authors declare the following financial interests/personal relationships which may be considered as potential competing interests: Konstantin G. Zloshchastiev reports financial support was provided by National Research Foundation.

Data availability

Data will be made available on request.

Acknowledgments

The authors are grateful to participants of the conference "Computer simulations in Physics and beyond" (CSP2020) for stimulating discussions and remarks [40]. Computing facilities at the Centre for High Performance Computing (CHPC) in Cape Town were used to perform all simulations in this study. K.G.Z.'s research is supported by Department of Higher Education and Training of South Africa and in part by National Research Foundation of South Africa (Grant Numbers 95965 and 132202). M.L.'s work is supported by the National Research Foundation, South Africa as part of its Rated Researcher programme.

References

[1] G. Rosen, Particlelike solutions to nonlinear complex scalar field theories with positive-definite energy densities, J. Math. Phys. 9 (1968) 996.
[2] I. Bialynicki-Birula, J. Mycielski, Nonlinear wave mechanics, Ann. Phys., NY 100 (1976) 62.
[3] H. Buljan, A. Šiber, M. Soljačić, T. Schwartz, M. Segev, D.N. Christodoulides, Incoherent white light solitons in logarithmically saturable noninstantaneous nonlinear media, Phys. Rev. E 68 (2003) 036607.
[4] K. Yasue, Quantum mechanics of nonconservative systems, Ann. Phys., NY 114 (1978) 479.
[5] J.D. Brasher, Nonlinear wave mechanics, information theory, and thermodynamics, Internat. J. Theoret. Phys. 30 (1991) 979.
[6] D. Schuch, Nonunitary connection between explicitly time-dependent and nonlinear approaches for the description of dissipative quantum systems, Phys. Rev. A 55 (1997) 935.
[7] S. De Martino, M. Falanga, C. Godano, G. Lauro, Logarithmic Schrödinger-like equation in magma, Europhys. Lett. 63 (2003) 472.
[8] K.G. Zloshchastiev, Logarithmic nonlinearity in theories of quantum gravity: Origin of time and observational consequences, Gravit. Cosmol. 16 (2010) 288.
[9] K.G. Zloshchastiev, Spontaneous symmetry breaking and mass generation as built-in phenomena in logarithmic nonlinear quantum theory, Acta Phys. Polon. 42 (2011) 261.
[10] A.V. Avdeenkov, K.G. Zloshchastiev, Quantum Bose liquids with logarithmic nonlinearity: Self-sustainability and emergence of spatial extent, J. Phys. B: At. Mol. Opt. Phys. 44 (2011) 195303.
[11] K.G. Zloshchastiev, Volume element structure and roton-maxon-phonon excitations in superfluid helium beyond the Gross–Pitaevskii approximation, Eur. Phys. J. B 85 (2012) 273.
[12] K.G. Zloshchastiev, On the dynamical nature of nonlinear coupling of logarithmic quantum wave equation, Everett–Hirschman entropy and temperature, Z. Naturf. a 73 (2018) 619.
[13] K.G. Zloshchastiev, Nonlinear wave-mechanical effects in korteweg fluid magma transport, Europhys. Lett. (EPL) 122 (2018) 39001.
[14] K.G. Zloshchastiev, Temperature-driven dynamics of quantum liquids: Logarithmic nonlinearity, phase structure and rising force, Internat. J. Modern Phys. B 33 (2019) 1950184.
[15] T.C. Scott, K.G. Zloshchastiev, Resolving the puzzle of sound propagation in liquid helium at low temperatures, Low Temp. Phys. 45 (2019) 1231.
[16] K.G. Zloshchastiev, An alternative to dark matter and dark energy: Scale-dependent gravity in superfluid vacuum theory, Universe 6 (2020) 180.
[17] K.G. Zloshchastiev, Superfluid stars and Q-balls in curved spacetime, Low Temp. Phys. 47 (2021) 89.
[18] K.G. Zloshchastiev, Acoustic oscillations in cigar-shaped logarithmic Bose–Einstein condensate in the Thomas–Fermi approximation, Internat. J. Modern Phys. B 35 (2021) 2150229.
[19] M. Kraiev, K. Domina, V. Kraieva, K.G. Zloshchastiev, Logarithmic wave-mechanical effects in polycrystalline metals: Theory and experiment, Indian J. Phys. 96 (2022) 2385.
[20] J.E. Dunn, J.B. Serrin, On the thermomechanics of interstitial working, Arch. Ration. Mech. Anal. 88 (1985) 95–133.
[21] D.M. Anderson, G.B. Mc Fadden, A.A. Wheeler, Diffuse-interface methods in fluid mechanics, Annu. Rev. Fluid Mech. 30 (1998) 139.
[22] B. Janovic, in: D. Henderson (Ed.), Fundamentals of Inhomogeneous Fluids, CRC Press, Boca Raton, 1992.
[23] D.M. Heyes, G. Rickayzen, J.G. Powles, Monte Carlo simulations of fluids whose particles interact with a logarithmic potential, J. Chem. Phys. 128 (2008) 134503.
[24] J.G. Powles, G. Rickayzen, D.M. Heyes, Purely viscous fluids, Proc. R. Soc. Lond. Ser. A Math. Phys. Eng. Sci. 455 (1999) 3725–3742.
[25] M.P. Allen, D.J. Tildesley, Computer Simulations of Liquids, Oxford Clarendon Press, 1987.
[26] A.Z. Panagiotopoulos, Direct determination of phase coexistence properties of fluids by Monte Carlo simulation in a new ensemble, Mol. Phys. 61 (1987) 813–826.
[27] A.Z. Panagiotopoulos, N. Quirke, M. Stapleton, D.J. Tildesley, Phase equilibria by simulation in the Gibbs ensemble, Mol. Phys. 63 (1988) 527–545.
[28] N. Metropolis, A.W. Rosenbluth, M.N. Rosenbluth, A.H. Teller, E. Teller, Equation of state calculations by fast computing machines, J. Chem. Phys. 21 (1953) 1087.
[29] M.G. Martin, MCCCS towhee: a tool for Monte Carlo molecular simulation, Mol. Simul. 39 (2013) 1212–1222.
[30] S. Yashonath, C.N.R. Rao, A Monte Carlo study of crystal structure transformations, Mol. Phys. 54 (1985) 245–251.
[31] H. Sun, COMPASS: An ab initio force-field optimized for condensed-phase applications – overview with details on alkane and benzene compounds, J. Phys. Chem. B 102 (1998) 7338–7364.
[32] A.A. Samoletov, C.P. Dettmann, M.A.J. Chaplain, Thermostats for slow configurational modes, J. Stat. Phys. 121 (2007) 1321–1336.
[33] L. Verlet, Computer experiments on classical fluids. I. Thermodynamical properties of Lennard–Jones molecules, Phys. Rev. 159 (1964) 98.
[34] Dassault Systémes BIOVIA, Materials Studio 2018, Dassault Systémes, San Diego, 2017.
[35] A. Einstein, Über die von der molekularkinetischen theorie der wärme geforderte bewegung von in ruhenden flüssigkeiten suspendierten teilchen, Ann. Phys. (Berlin) 17 (1905) 549.
[36] J.R. Fried, M. Sadat-Akhavi, J.E. Mark, Molecular simulation of gas permeability: poly (2, 6-dimethyl-1, 4-phenylene oxide), J. Membr. Sci. 149 (1998) 115–126.
[37] R.E. Zeebe, On the molecular diffusion coefficients of dissolved CO_2, HCO_3^-, and CO_3^{2-} and their dependence on isotopic mass, Geochim. Cosmochim. Acta 75 (2011) 2483–2498.
[38] V.N. Ryzhov, E.E. Tareyeva, Yu.D. Fomin, E.N. Tsiok, E.S. Chumakov, Renormalization group study of the melting of a two-dimensional system of collapsing hard disks, Theoret. Math. Phys. 191 (2017) 842–855.
[39] M. Edmonds, A. Brett, R.A. Herd, M.C.S. Humphreys, A. Woods, Magnetite-bubble aggregates at mixing interfaces in andesite magma bodies, Geol. Soc. Spec. Publ. 410 (2015) 95–121.
[40] M. Lasich, K.G. Zloshchastiev, Particle size and phase equilibria in classical logarithmic fluid, J. Phys. Conf. Ser. 1740 (2021) 012042.